Journal of Nuclear Materials 385 (2009) 615–622

Contents lists available at ScienceDirect

Journal of Nuclear Materials

journal homepage: www.elsevier.com/locate/jnucmat

Evolution of the nanostructure of VVER-1000 RPV materials under neutron irradiation and post irradiation annealing

M.K. Miller [a,*], A.A. Chernobaeva [b], Y.I. Shtrombakh [b], K.F. Russell [a], R.K. Nanstad [a], D.Y. Erak [b], O.O. Zabusov [b]

[a] Materials Science and Technology Division, Oak Ridge National Laboratory, P.O. Box 2008, Oak Ridge, TN 37831-6136, USA
[b] Russian Research Center, Kurchatov Institute, Moscow, Russia

ARTICLE INFO

Article history:
Received 20 August 2008
Accepted 18 January 2009

PACS:
61.80.Hg

ABSTRACT

A high nickel VVER-1000 (15Kh2NMFAA) base metal (1.34 wt% Ni, 0.47% Mn, 0.29% Si and 0.05% Cu), and a high nickel (12Kh2N2MAA) weld metal (1.77 wt% Ni, 0.74% Mn, 0.26% Si and 0.07% Cu) have been characterized by atom probe tomography to determine the changes in the microstructure during neutron irradiation to high fluences. The base metal was studied in the unirradiated condition and after neutron irradiation to fluences between 2.4 and 14.9 $\times$ 10^{23} m^{-2} (E > 0.5 MeV), and the weld metal was studied in the unirradiated condition and after neutron irradiation to fluences between 2.4 and 11.5 $\times$ 10^{23} m^{-2} (E > 0.5 MeV). High number densities of ~2-nm-diameter Ni-, Si- and Mn-enriched nanoclusters were found in the neutron irradiated base and weld metals. No significant copper enrichment was associated with these nanoclusters and no copper-enriched precipitates were observed. The number densities of these nanoclusters correlate with the shifts in the $\Delta T_{41\ J}$ ductile-to-brittle transition temperature. These nanoclusters were present after a post irradiation anneal of 2 h at 450 °C, but had dissolved into the matrix after 24 h at 450 °C. Phosphorus, nickel, silicon and to a lesser extent manganese were found to be segregated to the dislocations.

Published by Elsevier B.V.

1. Introduction

The long term operation of nuclear power plants is currently under consideration for almost all types of reactors including the water-moderated VVER-1000 type reactors. The prediction and evaluation of radiation embrittlement for reactor pressure vessel (RPV) materials is of particular importance for ensuring the safe operation of VVER-type nuclear power plants during their design and over their planned lifetime. In order to predict the embrittlement of steels used in these reactors, it is necessary to understand the micro-processes that occur under irradiation.

The embrittlement of reactor pressure vessel materials under irradiation is estimated by a transition temperature shift (ΔT_k). $\Delta T_k = T_k - T_{k0}$, where T_k is the transition temperature in the irradiated condition, and T_{k0} is the transition temperature in the unirradiated condition. According to the Russian Guide [1] the functional dependence of ΔT_k versus fast neutron dose is evaluated from the following formula:

$$\Delta T_F^{RG} = A_F \times (F/F_0)^{1/3}, \quad (1)$$

where

- F is fast neutron fluence with E > 0.5 MeV, m^{-2},
- $F_0 = 10^{22}$ m^{-2},
- A_F is radiation embrittlement coefficient, °C,
- $A_F = 23$ for the steel of 15Kh2NMFAA grade, and
- $A_F = 20$ for the welds of 15Kh2NMFAA grade.

The data concerning the transition temperature shifts under irradiation obtained during the last 10–15 years were based on tests of VVER-1000 RPV materials after irradiation in special channels in the VVER-1000 reactor. The data have shown, as suggested in [2], that the dependences expressed in Eq. (1) are not always conservative, especially for materials with high nickel content (i.e., more than 1.5% Ni) [3–5]. Moreover, the nickel content of most operating VVER-1000 RPV welds exceeds 1.5% Ni and, in some cases it even reaches 1.9% Ni. Thus, the development of an adequate model for $\Delta T_k = f(fluence)$ at the present time is a continuing issue.

The main advantage of any adequate model is the ability to reliably predict the degree of embrittlement. The forecasting quality of the model improves when the model is based on an understanding of the micro-processes that occur under irradiation and that are responsible for controlling the mechanical properties, including hardening and embrittlement. Therefore, a reliable description of the evolution of the microstructure during irradiation is essential.

The microstructures of several neutron irradiated VVER-1000 materials have been characterized by electron microscopy,

* Corresponding author.
E-mail address: millermk@ornl.gov (M.K. Miller).

0022-3115/$ - see front matter Published by Elsevier B.V.
doi:10.1016/j.jnucmat.2009.01.299

fractography and Auger electron spectroscopy (AES) [6–12]. These studies have revealed dislocation loops, precipitates and phosphorus grain boundary segregation under irradiation. However, the chemical composition of precipitates was not established.

Progress in understanding the processes of nanostructure evolution and material degradation mechanisms under irradiation is due in part to the development of higher resolution methods for microstructural examination, such as atom probe tomography (APT). The majority of APT studies have been performed on Western RPV steels and these studies have been reviewed recently [13–16]. In addition, several studies have been performed on forgings and weld metals from VVER-440 and VVER-1000 reactors [17–25]. As there are significant differences in the chemical compositions of Western and Russian RPV steels, a direct comparison of a significant proportion of previous APT results may not be applicable to VVER-1000 RPV materials. For example, the manganese and copper contents in the VVER-1000 steels is lower, and the nickel content is much higher. Higher nickel weld metals have been shown to have an increased sensitivity to neutron irradiation at high fluences [3–5], as accounted for, e.g., in the US Regulatory Guide 1.99, Revision 2 [26,27].

In this APT study, the evolution of the nanostructure of a high nickel base (1.34% Ni, 0.47% Mn, 0.05% Cu) and weld (1.77% Ni, 0.74% Mn, 0.07% Cu) material with a Russian VVER-1000 type reactor composition has been characterized under high fluence irradiation and post irradiation annealing (PIA). In a preliminary study of the same base and weld materials, ultrafine (1.8-nm-diameter) nickel-, manganese- and silicon-enriched nanoclusters were observed in materials that were neutron irradiated in the Ford test reactor to a total fluence of $1.4 \times 10^{23}\ m^{-2}$ ($E > 1$ MeV) [$2.4 \times 10^{23}\ m^{-2}$($E > 0.5$ MeV)] at a temperature of 288 °C [16]. The main distinction of the research reported in this paper is that the steels were studied after irradiation to several different states within a higher range of fluences, i.e., ~2.4 to $12 \times 10^{23}\ m^{-2}$ ($E > 0.5$ MeV),[1] and after PIA.

2. Materials and experimental procedures

In the framework of the International Atomic Energy Agency (IAEA) Coordinated Research Project (CRP) 'Effects of Nickel on Irradiation Embrittlement of Light Water Reactor Pressure Vessel (RPV) Steels', two low copper materials, a base metal with 1.34 wt% Ni and a weld metal with 1.77% Ni, prepared by standard VVER-1000 technology procedures, were selected for investigation [2]. The chemical compositions of these materials are presented in Table 1.

Several laboratories from different countries have irradiated and tested these materials. Mechanical property characterizations of both materials in the unirradiated state were performed by Charpy V-notch (CVN) impact tests at the Russian Research Center Kurchatov Institute (RRC KI) and at the Oak Ridge National Laboratory (ORNL). Transition temperatures were assessed both at ORNL and at RRC KI. Statistical analysis of the RRC-KI/ORNL joint data file for each material was performed using the Chow test.

The Chow Test evaluates the hypothesis that transition curves plotted for two different samples are coincident (i.e., corresponding coefficients in regression equations are equal). If the P-value of the Chow Test $\geqslant 0.05$, the hypothesis is not rejected at the 5% significance level, hence the coefficients are equal. For the joint data file, the Chow Test shows that the P-value is 0.62 for base metal and 0.62 for weld metal. This fact indicates the possibility for analysis of the data obtained by both ORNL and RRC KI, including post irradiation data, as a whole data file.

[1] Hereafter all fluences are stated in values of E >0.5 MeV.

Table 1
Chemical composition of the investigated VVER-1000 base and weld materials.

Element	Base metal		Weld metal	
Balance Fe	wt%	at.%	wt%	at.%
C	0.17	0.78	0.08	0.28
Si	0.29	0.59	0.26	0.65
Mn	0.47	0.46	0.74	0.81
Cr	2.24	2.34	1.80	1.93
Ni	1.34	1.19	1.77	1.69
Cu	0.05	0.04	0.07	0.06
S	0.014	0.024	0.013	0.023
P	0.009	0.014	0.006	0.009
V	0.09	0.11	0.02	0.02
Mo	0.51	0.30	0.64	0.33

Tensile tests of the base and weld metals in the unirradiated condition and after neutron irradiation were performed at RRC KI. Some neutron irradiations of CVN specimens of base and weld metals were performed in the HSSI Irradiation, Annealing, Reirradiation (IAR) facility at the University of Michigan Ford Reactor. Additionally, neutron irradiations were performed in a VVER-1000 reactor at the RRC KI. The irradiation conditions for these experiments are summarized in Table 2. The values of doses and dose rates given in Table 2 correspond to the arithmetical means for each group of specimens.

The hardening under irradiation was assessed by testing tensile specimens using the value of yield stress increase ($\Delta R_{P0.2}$), where $\Delta R_{P0.2} = \Delta R_{P0.2} - \Delta R_{P0.20}$, and $\Delta R_{P0.2}$ and $\Delta R_{P0.20}$ are the yield stresses in the irradiated and unirradiated states, respectively.

Atom probe tomography was used to investigate the changes in the nanostructure of each material after neutron irradiation to different fluences at a temperature of 288–290 °C. A summary of the irradiation conditions of the base and weld metals examined in the APT investigations are presented in Table 3. The stability of the microstructural features was also investigated after two PIA treatments. Both PIA treatments of 2 and 24 h at 450 °C were performed on $0.5 \times 0.5 \times 10$ mm blanks in an inert argon atmosphere.

The atom probe tomography characterizations were performed in the ORNL local electrode atom probe (LEAP®) [28,29]. Atom probe needle-shaped specimens were electropolished from $0.5 \times 0.5 \times 10$ mm blanks cut from bulk material. The standard 2-stage electropolishing procedure was used with a mixture of 25% perchloric acid in acetic acid for the double layer stage 1 and a solution of 2% perchloric acid in 2-butoxyethanol for stage 2 [30]. Specimens were also repolished with the loop method [29,30]. The experimental parameters used for these APT characterizations were a specimen temperature of 60 K, a pulse fraction of 0.2, and a pulse repetition rate of 200 kHz in voltage-pulsed mode. All atom probe concentration estimates in this paper are given in atomic percent. Statistical analysis of the size, number density and composition of the nanoclusters was performed with the maximum separation method [29,31] and the envelope method [29]. A detailed discussion of the applications of these methods to the characterization of ultrafine precipitates in RPV steels has been reported recently [16]. It should be emphasized that the estimated composition of features in the ~1–2 nanometer size range typically observed in neutron irradiated pressure vessel steels is strongly dependent on the precise definition of the location of the interface between the precipitate/nanocluster and the matrix, the assignment of the solvent (Fe) atoms in the interface region to the phases, and the shape and sharpness of the solute concentration profiles. The parameters used were a maximum separation distance, d_{max}, of 0.6 nm, a minimum number of atoms, n_{min} of 10 atoms, a grid spacing of 0.1 nm, and ranges for Cu, Mn and Ni_{30} atoms. The nickel concentration was corrected with the use of the natural abundances of the isotopes.

Table 2
Neutron irradiation conditions for the VVER-1000 RPV materials studied.

Material	Place of irradiation	T_{Irr} (°C)	$F(E > 0.5\ MeV) \times 10^{23}\ m^{-2}$	Flux $(E > 0.5\ MeV) \times 10^{16}\ m^{-2}s^{-1}$
Base metal	Ford Reactor	288 ± 2	2.4	0.5
	VVER-1000	290 ± 2	9.5	2–4
	VVER-1000	290 ± 2	14.9	2–4
Weld metal	Research reactor	288 ± 2	2.4	0.5
	VVER-1000	290 ± 2	3.2	2–4
	VVER-1000	290 ± 2	5.1	2–4
	VVER-1000	290 ± 2	6.8	2–4
	VVER-1000	290 ± 2	11.5	2–4

Table 3
Summary of the neutron irradiation and post irradiation annealing conditions used for the APT investigation of the base and weld metals. All fluences are $E > 0.5$ MeV.

Material	State
Base Metal	Irradiated to $2.4 \times 10^{23}\ m^{-2}$
	Irradiated to $9.5 \times 10^{23}\ m^{-2}$
	Irradiated to $14.9 \times 10^{23}\ m^{-2}$
	Irradiated to $14.9 \times 10^{23}\ m^{-2}$ + Annealed for 2 h at 450 °C
	Irradiated to $14.9 \times 10^{23}\ m^{-2}$ + Annealed for 24 h at 450 °C
Weld Metal	Irradiated to $2.4 \times 10^{23}\ m^{-2}$
	Irradiated to $5.1 \times 10^{23}\ m^{-2}$
	Irradiated to $6.8 \times 10^{23}\ m^{-2}$
	Irradiated to $11.5 \times 10^{23}\ m^{-2}$
	Irradiated to $11.5 \times 10^{23}\ m^{-2}$ + Annealed for 2 h at 450 °C
	Irradiated to $11.5 \times 10^{23}\ m^{-2}$ + Annealed for 24 h at 450 °C

3. Results and discussion

The test results of Charpy V-notch (CVN) base and weld metal specimens in the unirradiated condition are presented in Fig. 1. The irradiation-induced changes in the mechanical properties are presented in Table 4 and Figs. 2 and 3. Following irradiation to a fluence of $2.4 \times 10^{23}\ m^{-2}$ ($E > 0.5$ MeV), the transition temperature shifts are relatively small and are approximately the same for base and weld metals. As expected, the embrittlement increases with fluence for both base and weld metals. The embrittlement rate of the weld metal is much greater than twice that for the base metal. Test results of the CVN specimens show a linear dependence versus fluence with goodness of fit of $R^2 = 0.99$ for the weld metal. A linear fit for the more limited number of data for the base metal yielded a lower goodness of fit of only 0.88 and appear to better fit a parabolic dependency. A linear type of dependence was previously suggested [32].

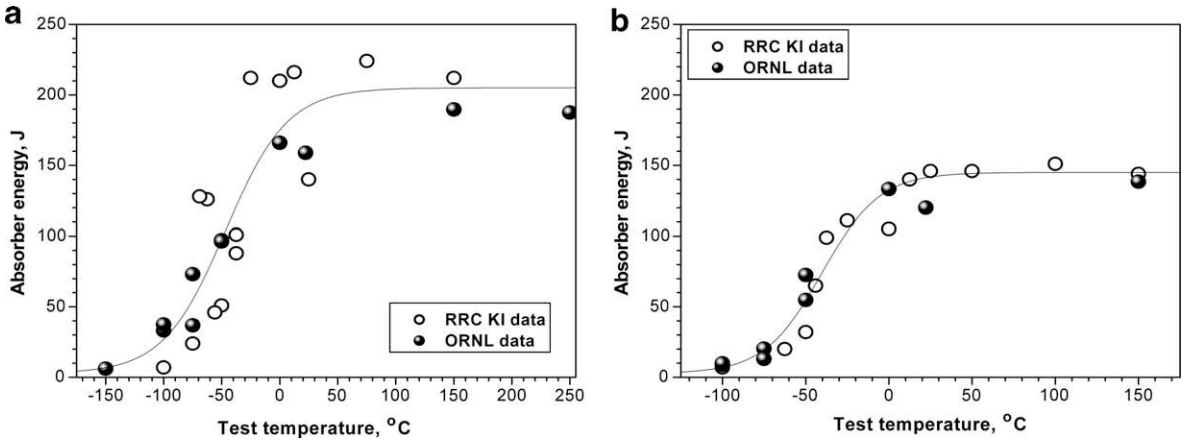

Fig. 1. Charpy impact test results of the VVER-1000 RPV (a) base metal and (b) weld metal in the unirradiated condition.

Table 4
Values of yield strength, $\Delta R_{P0.2}$, and CVN transition temperatures, T_k, for the base and weld metals in the unirradiated and neutron irradiated conditions.

Material	$F(E > 0.5\ MeV), \times 10^{22}\ m^{-2}$	$R_{P0.2}$, MPa	$\Delta R_{P0.2}$, MPa	T_K, °C	ΔT_K, °C
Base Metal	0	599		−81	
	24	–	–	−51	30
	95	693	94	−16	65
	149	–	–	−4	77
Weld Metal	0	536		−59	
	24	–	–	−24	35
	32	612	76	−16	43
	51	623	87	5	64
	56	641	105		
	68	–	–	29	88
	115	–	–	95	154

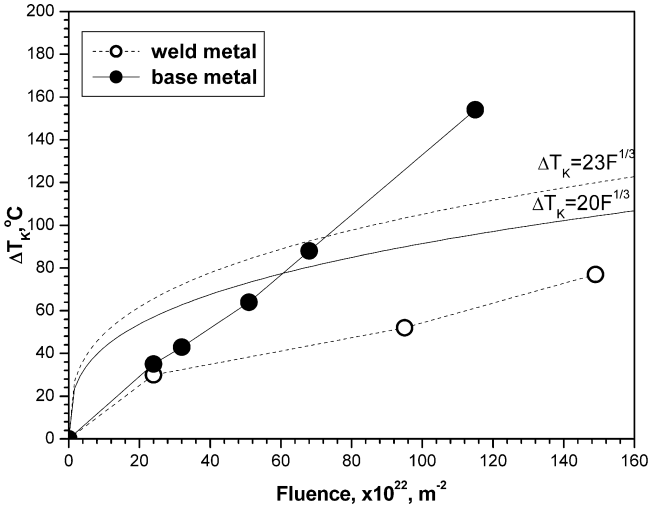

Fig. 2. Transition temperature shift versus neutron dose, for: (a) base metal and (b) weld metal. The curves labeled with ΔT_k are those from the Russian Standard [1].

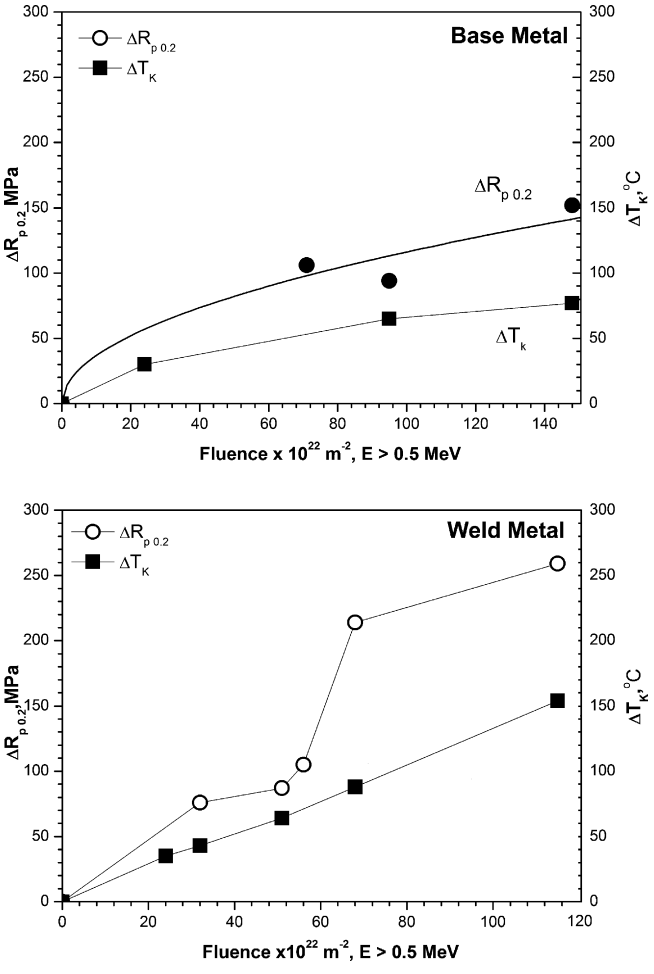

Fig. 3. $\Delta R_{P0.2}$ and the corresponding ΔT_k values for base and weld metals for the different fluences.

Comparison of ΔT_k experimental values with the reference dependence, shown in Fig. 2, indicates that the reference dependence does not account for the specific chemical compositions of the steels.

It is known that nickel and manganese have the most influence on embrittlement for materials with low copper and phosphorous and high nickel (>1%) contents [3–5]. The results given in Table 4 and in Fig. 2 show that increases of nickel content from 1.34 to 1.77 wt%, and manganese from 0.47 to 0.74 wt% leads to an ~3 times increase in transition temperature.

The values of $\Delta R_{P0.2}$ and the corresponding ΔT_k values are given in Table 4 and Fig. 3. The ratios of hardening to transition temperature shift $\Delta T_k/\Delta R_{P0.2}$ are ~0.7 and 0.6–0.7 for base and weld metals, respectively. As these ratios are practically equal for the weld and base metal and the similarity of $\Delta R_{P0.2}$ and the corresponding ΔT_k of the weld metal (Fig. 3(b)) indicate that hardening is the basic mechanism of embrittlement under irradiation to doses of $\sim 0.5–1.0 \times 10^{24}$ m^{-2}. These values are similar to those found in studies for western RPV steels by Odette [33], Nanstad [34], and Sokolov [35] for lower dose irradiation.

Typical selected volume atom maps of the base and weld metal for the different fluences are shown in Figs. 4 and 5, respectively. High number densities of ~2-nm-diameter, roughly spherical, Ni-, Mn- and Si-enriched nanoclusters are evident in both the base and weld metals. In order to improve the visibility of the nanoclusters for these relatively high solute contents, these atom maps were 10-nm-thick volumes extracted from the significantly larger sampled volumes. The atom maps indicated that the nanoclusters are not significantly enriched in copper. It should be noted that significant proportions of atoms shown in the copper and phosphorus maps are from random background noise events (e.g., the background noise levels are less than ~700 appm for Cu and less than ~200 appm for P) which cannot be removed on an atom by atom basis as it is impossible to distinguish an individual atom from a noise count. A high resolution atom map of three nanoclusters in

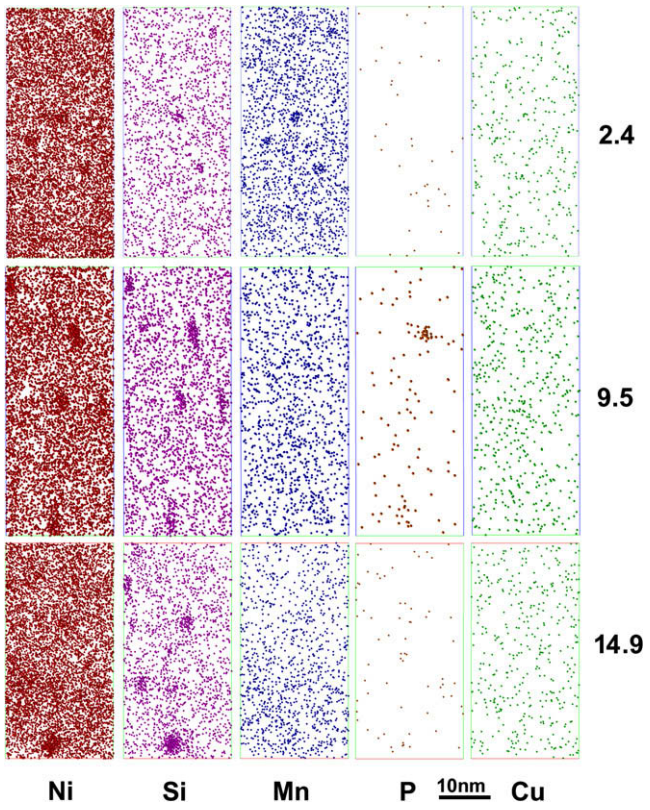

Fig. 4. Atom maps of the Ni-, Si-enriched nanoclusters in the base metal for the different fluences. Each atom map is 10 nm thick. Fluence is in units of 10^{23} m^{-2} ($E > 0.5$ MeV). Significant proportions of atoms shown in the copper and phosphorus maps are from random background noise.

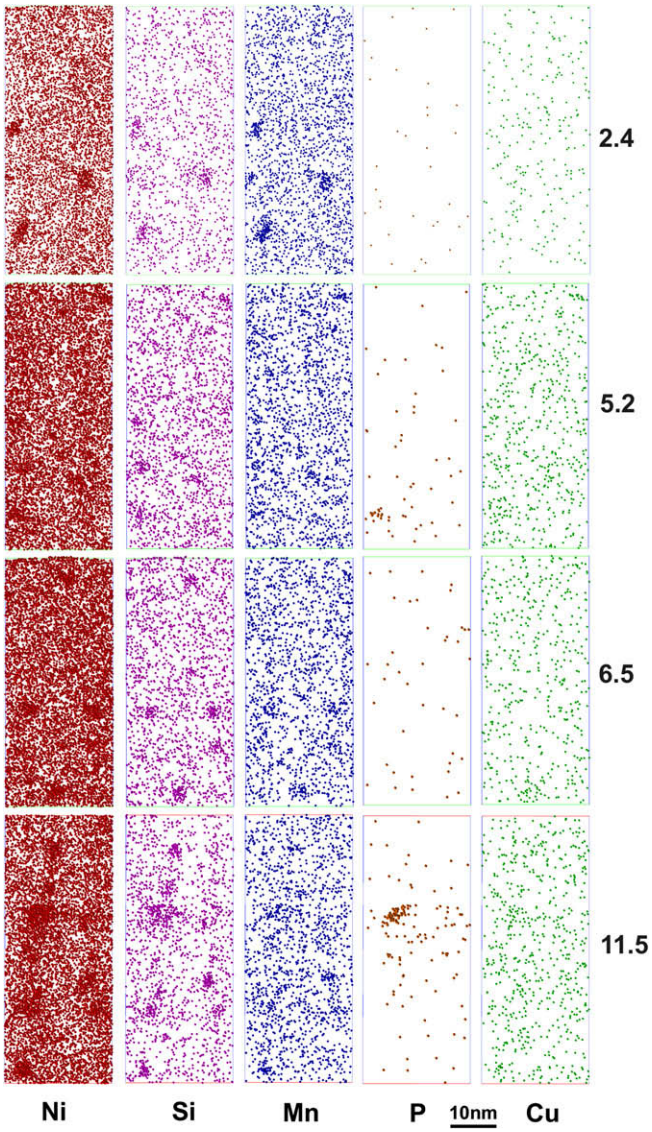

Fig. 5. Atom maps of the Ni-, Si- and Mn-enriched nanoclusters in the weld metal for different fluences. Each atom map is 10 nm thick. The high phosphorus regions correspond to a dislocation. Fluence is in units of 10^{23} m^{-2} ($E > 0.5$ MeV). Significant proportions of atoms shown in the copper and phosphorus maps are from random background noise.

the highest fluence weld metal (fluence = 11.5×10^{23} m^{-2}) indicating the ramified nature of the interface is shown in Fig. 6. The average radial concentration profiles constructed from the centers of mass of 30 nanoclusters revealed that they are only slightly enriched in copper, as shown in Fig. 7. However, the estimated copper level is substantially lower than that estimated in the body-centered-cubic (bcc) copper-enriched precipitates found in most neutron irradiated copper-containing RPV steels and copper-containing model alloys [13–16,36] including high nickel and medium and high copper steels, including a 1.2% Ni, 0.2% Cu weld from the Palisades reactor [25], a 1.72% Ni, 0.63% Cu weld, [31,37], and the 3.7% Ni, 0.08% Cu, A508 Gr4N forging steel [38–40]. Thus, these nanoclusters are distinctly different from the copper-enriched precipitates. The term nanocluster is used in this paper primarily to distinguish them from the bcc Cu-enriched precipitates found in other RPV steels. No experimental data are currently available on the crystal structure of these Ni-, Mn- and Si-enriched nanoclusters.

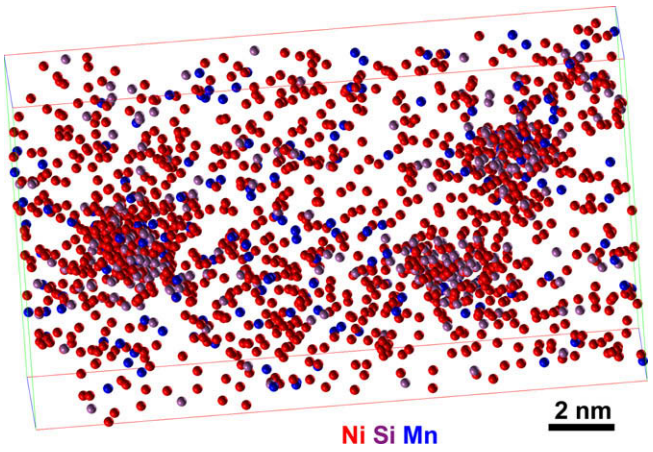

Fig. 6. High resolution atom map of three Ni-, Si- and Mn-enriched nanoclusters in the highest fluence weld metal (fluence = 11.5×10^{23} m^{-2} ($E > 0.5$ MeV)) showing the distribution of the Ni, Si and Mn atoms.

The average size (i.e., radius of gyration) and number density of the nanoclusters for the base and weld metals for the different fluences, are summarized in Table 5. The variations of the size and number density with fluence are shown in Figs. 8 and 9, respectively. No statistically significant increase in the average radius of gyration was found with increasing fluence. A similar result was found for the precipitates in a low copper steel from the Chooz reactor [41]. The size of Cu-enriched precipitates increases under irradiation [42–44].

The typical number of atoms in the nanoclusters was less than 100. The size distribution of these nanoclusters for the highest fluence weld metal is shown in Fig. 10. The distribution was almost symmetrical about the mean size with a small tail in the higher size range.

Local inhomogeneities in the number density of nanoclusters on the sub-micron scale and from specimen to specimen produces large scatter in the data and therefore precluded a detailed analysis of the number densities. The inhomogeneities were most pronounced in the low dose base metal. However, the general trends were apparent. In both the base and weld metals, higher irradiation doses generated higher number densities of Ni-, Mn- and Si-enriched nanoclusters. A similar result was found for the precipitates in a low copper steel from the Chooz reactor [41]. The density of Cu-rich precipitates, however, exhibits only a minimal increase under irradiation [42,45].

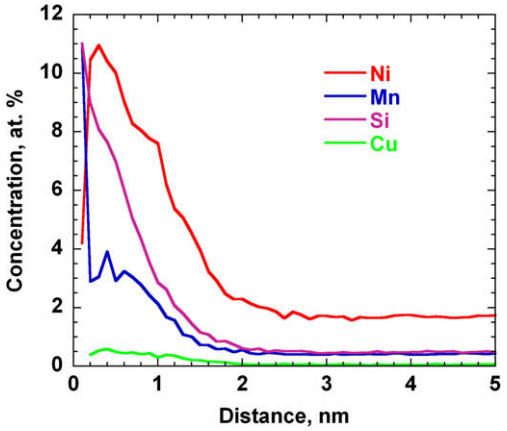

Fig. 7. The average radial concentration profiles of 30 nanoclusters constructed from the center-of-mass of each of the nanoclusters in the highest fluence weld metal (fluence = 11.5×10^{23} m^{-2} ($E > 0.5$ MeV)). Enrichments of Ni, Si and Mn are evident in the nanoclusters.

Table 5
Number densities and sizes of Ni-, Si- and Mn-enriched nanoclusters for the different neutron doses as estimated from atom probe analyses with the maximum separation method.

Material	Fluence, $\times 10^{22}$ m^{-2} ($E > 0.5$ MeV)	Number density $\times 10^{24}$, m^{-3}	Size, nm
Base Metal	24	0.7	0.85 ± 0.2
	95	1.1	0.91 ± 0.2
	149	1.8	0.93 ± 0.2
Weld Metal	24	0.3	0.77 ± 0.2
	52	1.6	0.87 ± 0.2
	65	2.6	0.93 ± 0.2
	115	2.9	0.90 ± 0.2

The number density increase correlates with the increased shifts in the ductile-to-brittle transition data observed in the Charpy data at least up to a dose of $\sim 6 \times 10^{23}$ m^{-2} for the weld metal. At higher doses the rate of ΔT_k for WM does not decrease in comparison with density increase.

For the highest doses in which the inhomogeneities were less, approximately a factor of two higher number density of nanoclusters was observed in the weld metal compared to the base metal. This increase correlates with the higher nickel and manganese contents of the weld metal.

The composition of the nanoclusters was estimated with the maximum separation envelope method. Due to the overlap of the

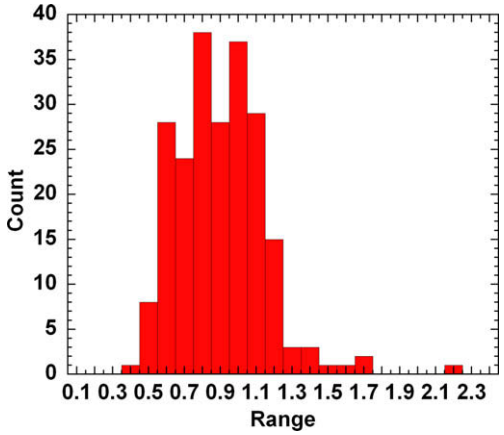

Fig. 8. The size distribution of the Ni-, Si-, and Mn-enriched nanoclusters in the highest fluence weld metal (fluence = 11.5×10^{23} m^{-2} ($E > 0.5$ MeV)).

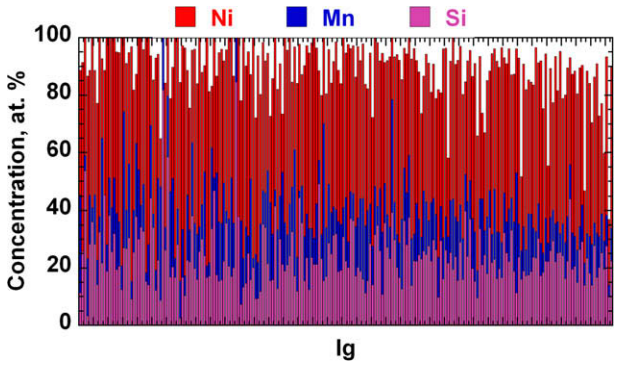

Fig. 9. The compositions of the Ni-, Si-, and Mn-enriched nanoclusters in the highest fluence weld metal (fluence = 11.5×10^{23} m^{-2} ($E > 0.5$ MeV)), as estimated by the maximum separation envelope method. The balance of these concentrations is predominantly iron. The data are sorted in terms of increasing radius of gyration.

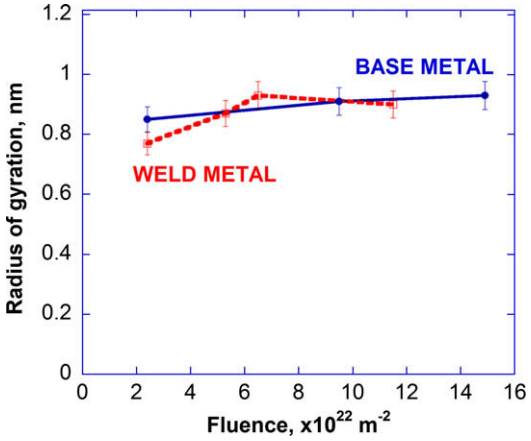

Fig. 10. The variation in the size of the Ni-, Si- and Mn-enriched nanoclusters in the base and weld metals with fluence. No statistically significant change in size is evident.

$_{58}Fe^{2+}$ and $_{58}Ni^{2+}$ isobars in the atom probe data, the analysis was performed with a d_{max} parameter of 0.6 nm for the combined $_{60}Ni^{2+}$, Mn^{2+} and Si^{2+} isobars and then scaled to the full nickel concentration. A cut off value of 10 atoms was used for the smallest agglomeration of atoms considered to be a nanocluster in order to eliminate random fluctuations. It should be noted that the envelope algorithm is extremely aggressive in removing the matrix atoms. Therefore, the ratios of the elements provide a more reliable estimate of the concentrations rather than the absolute levels. The results for the highest fluence weld metal are shown in Fig. 11. The composition data are arranged in order of increasing radius of gyration. No difference in composition was found in this limited size range. The average composition of the nanoclusters was estimated to be 50 ± 13 at.% Ni, 15 ± 9% Mn, 24 ± 11% Si, 0.14 ± 0.14% Cu, balance Fe for the highest fluence weld metal (fluence = 11.5×10^{23} m^{-2}) and 53 ± 19 at.% Ni, 9 ± 6% Mn, 25 ± 12% Si, 0.15 ± 0.15% Cu, balance Fe for the highest fluence base metal (fluence = 14.8×10^{23} m^{-2}). The large standard deviation in the estimated compositions is a reflection of the small number of atoms associated with each nanocluster. No statistical difference in the average compositions of the nanoclusters in the base and weld metals was observed. No statistical difference in the average compositions of the nanoclusters with fluence was observed. The Ni content of the nanoclusters was significantly higher than that of Si and Mn. Based on these composition estimates, the nanoclusters could be described as either having a $(Ni,Mn)_3Si$ stoichiometry

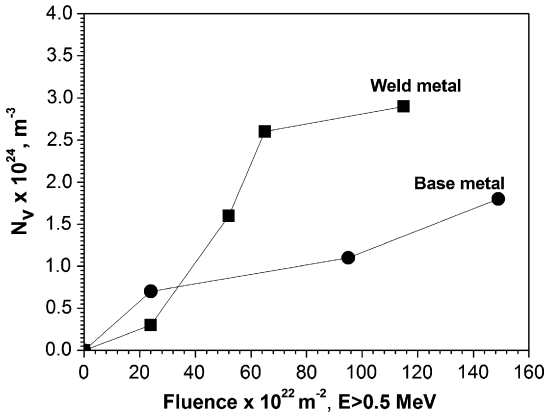

Fig. 11. The increase in number density of the Ni-, Si- and Mn-enriched nanoclusters in the base and weld metals with fluence.

or a concentrated solid solution of Ni, Si and Mn (such as could be produced by phase separation within a low temperature miscibility gap). There is no reliable phase diagram for this region of the multi-element system that takes into account the influence of the excess vacancies, etc. present during neutron irradiation. Atom probe tomography has shown previously that neutron irradiation significantly alters the position of the miscibility gap in the Fe–Cr spinodal system [46]. However, attempts to model these materials have indicated the formation of nanoclusters [47–49]. It was reported by Auger et al. [41] and Lambourne et al. [50], there is no difference in chemical composition after irradiation to different fluences.

Although the Ni-, Mn- and Si-enriched nanoclusters are in the same size range and number density as the copper-enriched precipitates previously reported in many irradiated RPV materials, their effect on the mechanical properties may differ depending on whether dislocations are able to cut through (modulus hardening) or bow around the nanoclusters. As shown by the ΔT_k results in Figs. 2 and 3, it is clear that the nanoclusters provide effective barriers to dislocation motion.

Phosphorus, nickel, silicon and to a lesser extent manganese were found to be segregated to the dislocations, as shown in the atom map in Fig. 12 for the highest fluence weld metal (fluence = 11.5×10^{23} m^{-2} ($E > 0.5$ MeV)). Unlike the copper-enriched precipitates, there was no evidence of preferential formation of the Ni-, Mn- and Si-enriched nanoclusters on dislocations. Phosphorus segregation to dislocations is a common feature in P-containing pressure vessel steels [13–16]. Manganese and silicon segregation to dislocations has also been observed in VVER-440 steels [21,22].

Atom maps of the highest fluence base and weld metals after the PIA treatments at 450 °C are shown in Figs. 13 and 14, respectively. The Ni-, Mn- and Si- enriched nanoclusters were still evident after the 2 h at 450 °C PIA treatment in both base and weld metals. Careful examination of the atom maps from the base metal revealed that the manganese in the nanoclusters was uniformly distributed. Preliminary DIffusion Controlled TRAnsformations (DICTRA) simulations have revealed that the diffusion rate of manganese is higher than that of nickel and silicon in iron and therefore, may indicate a faster dissolution of manganese. No nanoclusters and uniform distributions of Ni, Mn and Si were observed after the 24 h at 450 °C PIA treatment. The nickel content of the matrix was found to increase, indicating that the Ni-, Mn- and Si-enriched nanoclusters had dissolved rather than coarsened. This is contrasted with Cu-rich precipitates in RPV steels which exhibit coarsening following PIA treatment, but also exhibit a restoration of the toughness. This behavior indicates that PIA temperature of 450 °C for this composition is in a single phase region. This dissolution mechanism also suggests that the solute will form a new distribution of nanoclusters and consequential re-embrittlement on subsequent re-irradiation at the lower operating temperature of the VVER-1000 reactor.

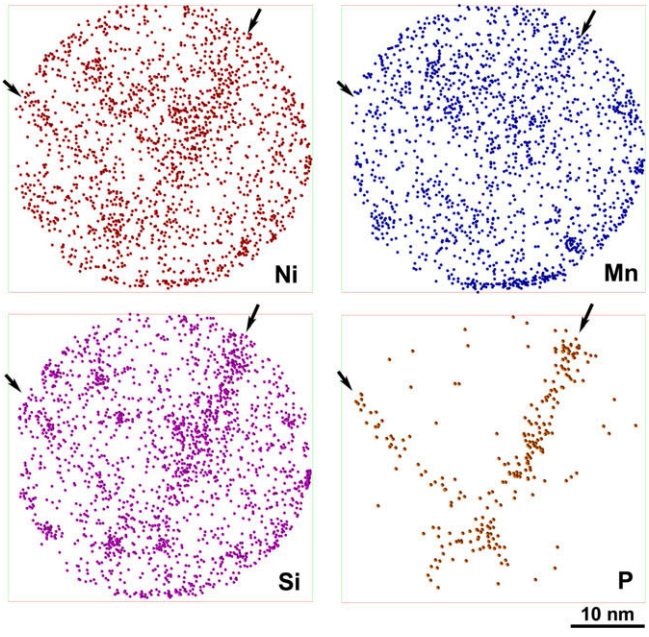

Fig. 12. Phosphorus, nickel, silicon and to a lesser extent manganese were found to be segregated to the dislocations in the highest fluence weld metal (fluence = 11.5×10^{23} m^{-2} ($E > 0.5$ MeV)) weld metal.

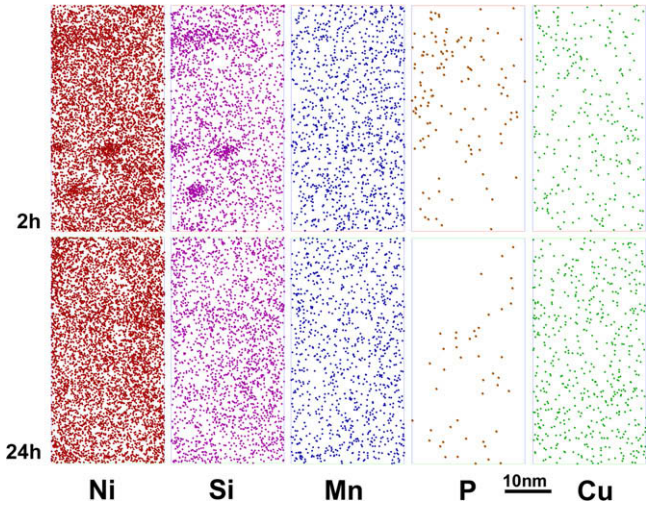

Fig. 13. Atom maps of the highest fluence base metal (fluence = 11.5×10^{23} m^{-2} ($E > 0.5$ MeV)) after the post irradiation annealing treatments of: (a) 2 and (b) 24 h at 450 °C. The nanoclusters were present after post irradiation annealing for 2 h but not after 24 h. Note the uniform manganese distribution in the 2 h PIA condition.

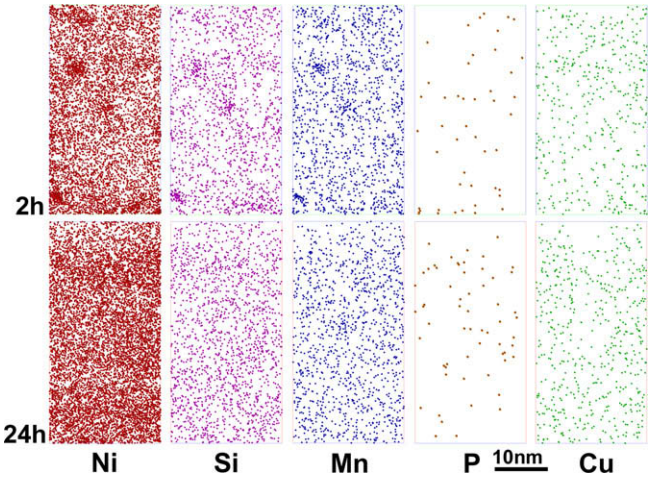

Fig. 14. Atom maps of the highest fluence weld metal (fluence = 14.9×10^{23} m^{-2} ($E > 0.5$ MeV)) after the post irradiation annealing treatments of: (a) 2 and (b) 24 h at 450 °C. The nanoclusters were present after post irradiation annealing for 2 h but not after 24 h.

4. Conclusions

The microstructures of a high nickel, low copper VVER-1000 base metal (1.34 wt% Ni, 0.47% Mn, 0.29% Si and 0.05% Cu), and a

high nickel, low copper weld metal (1.77 wt% Ni, 0.74% Mn, 0.26% Si and 0.07% Cu) have been characterized by atom probe tomography after neutron irradiation to fluences of up to 14.9×10^{23} m^{-3} and up to 11.5×10^{23} m^{-3} ($E > 0.5$ MeV), respectively. The fluence dependencies of $\Delta T_{41\ \text{J-ADJ}}$ values indicated increased radiation sensitivity of the higher nickel weld metal. High number densities of ~2-nm-diameter Ni-, Si- and Mn-enriched nanoclusters were found in the neutron irradiated base and weld metals. No copper enrichment was associated with these nanoclusters and no copper-enriched precipitates were observed. The number density of the nanoclusters increased during irradiation. However, the average size of nanoclusters did not change significantly. The composition of the nanoclusters in both base and weld metals was Fe- ~50% Ni, ~25% Si, ~10% Mn, and ~0.15% Cu. Given the local variability in these materials, there is a reasonable correlation between the shift in the Charpy mechanical property data with the number density of Ni-, Si- and Mn-enriched nanoclusters.

The increase in density, permanent size and chemical composition is strongly indicative that the nanoclusters are radiation induced features.

These nanoclusters were present after a post irradiation anneal of 2 h at 450 °C but had dissolved into the matrix after 24 h at 450 °C. Phosphorus, nickel, silicon and to a lesser extent manganese were found to be segregated to the dislocations.

Acknowledgments

The authors thank Dr S.S. Babu for providing the DICTRA calculations. Research at the Oak Ridge National Laboratory SHaRE User Facility was sponsored by Basic Energy Sciences, U.S. Department of Energy and by the Office of Nuclear Regulatory Research, U.S. Nuclear Regulatory Commission, under inter-agency agreement 1886-N695-3W and under contract DE-AC05-00OR22725 with UT-Battelle, LLC. Research at the Russian Research Center, Kurchatov Institute was performed under the International Science and Technology Center (ISTC) Project 3420.

References

[1] M. Energoatomizdat, Guide for strength analysis of the equipment and pipelines of nuclear power units, PNAE G-7-002-86, 1989.
[2] IAEA-TECDOC-1441, Effects of Nickel on Irradiation Embrittlement of Light Water Reactor Pressure Vessel Steels, IAEA, Vienna, Austria, 2005.
[3] Y.A. Nikolaev, Radiation embrittlement of VVER-1000 RPV steels, in: 18th International Conference on Structural Mechanics in Reactor Technology (SMiRT 18), Atomic Energy Press, Beijing, China, August 7–12, 2005, p. 935.
[4] A. Kryukov, D. Erak, L. Debarberis, F. Sevini, B. Acosta, Int. J. Pres. Ves. Pip. 79 (2002) 661.
[5] A.M. Kryukov, Y.A. Nikolaev, Nucl. Eng. Des. 195 (2000) 143.
[6] G. Brauer, K. Popp, Phys. Stat. Solidi A 102 (1987) 79.
[7] G. Brauer, W. Matz, L. Liszkay, B. Molnar, R. Krause, Mater. Sci. Forum 97–99 (1992) 379.
[8] G. Brauer, L. Liszkay, B. Molnar, R. Krause, Nucl. Eng. Des. 127 (1991) 47.
[9] G. Brauer, F. Eichhorn, Nucl. Eng. Des. 143 (1993) 301.
[10] B. Gurovich, E.A. Kuleshova, Y. Nikolaev, Y. Shtrombakh, The assessment of the contribution of different mechanisms to RPV materials irradiation embrittlement, RRC Kurchatov Institute preprint, 6025/11, 1997.
[11] B. Gurovich, E.A. Kuleshova, Yu.A. Nikolaev, Ya.I. Shtrombakh, J. Nucl. Mater. 246 (1997) 91.
[12] E.A. Kuleshova, B.A. Gurovich, Y.I. Shtrombakh, D.Y. Erak, J.V. Lavrenchuk, J. Nucl. Mater. 300 (2002) 127.
[13] M.K. Miller, M.G. Hetherington, M.G. Burke, Metall. Trans. 20A (1989) 2651.
[14] M.K. Miller, P. Pareige, M.G. Burke, Mater. Charact. 44 (2000) 235.
[15] P. Auger, P. Pareige, S. Welzel, J-C. Van Duysen, J. Nucl. Mater. 280 (2000) 331.
[16] M.K. Miller, K.F. Russell, J. Nucl. Mater. 371 (2007) 145. doi:10.1016/J.jnucmat.2007.05.003.
[17] M.K. Miller, R. Jayaram, P.J. Othen, G. Brauer, Atom probe field ion microscopy characterizations of VVER steels, in: R.E. Gold, E.P. Simonen (Eds.), Proceedings of 6th International Conference on Environmental Degradation of Materials in Nuclear Power Systems – Water Reactors, Minerals, Metals and Materials Society, 1993, p. 161.
[18] M.K. Miller, R. Jayaram, P.J. Othen, G. Brauer, Appl. Surf. Sci. 76/77 (1994) 242.
[19] M.K. Miller, R. Jayaram, K.F. Russell, J. Nucl. Mater. 225 (1995) 215.
[20] M.K. Miller, K.F. Russell, Appl. Surf. Sci. 94/95 (1996) 378.
[21] M.K. Miller, K.F. Russell, J. Kocik, E. Keilova, J. Nucl. Mater. 282 (2000) 83.
[22] M.K. Miller, K.F. Russell, J. Kocik, E. Keilova, Micron 32 (2001) 749.
[23] P. Pareige, B. Radiguet, A. Suvorov, M. Kozodaev, E. Krasikov, O. Zabusov, J.P. Massoud, Surf. Interface Anal. 36 (2004) 581.
[24] P. Pareige, B. Radiguet, R. Krummecih-Brangier, A. Barbu, O. Zabusov, M. Kozodaev, Philos. Mag. 85 (2005) 429.
[25] M.K. Miller, M.A. Sokolov, R.K. Nanstad, K.F. Russell, J. Nucl. Mater. 351 (2006) 187.
[26] Regulatory Guide 1.99, Radiation Embrittlement of Reactor Vessel Materials, Revision 2, US Nuclear Regulatory Commission, Washington, DC, May 1988.
[27] P.N. Randall, Basis for Revision 2 of the US Nuclear Regulatory Commission's Regulatory Guide 1.99, in: L.E. Steele (Ed.), Radiation Embrittlement in Nuclear Pressure Vessel Steels: An International Review, vol. 2, ASTM STP-909, 1987.
[28] T.F. Kelly, M.K. Miller, Rev. Sci. Instrum. 78 (2007) 031101.
[29] M.K. Miller, Atom Probe Tomography, Kluwar Academic/Plenum Publishing, New York, NY, 2000.
[30] M.K. Miller, G.D.W. Smith, Atom Probe Microanalysis: Principles and Applications to Materials Problems, Materials Research Society, Pittsburgh, PA, 1989.
[31] J.M. Hyde, C.A. English, in: G.E. Lucas, L. Snead, M.A. Kirk Jr., R.G. Elliman (Eds.), Proceedings of MRS 2000 Fall Meeting, Symposium R: Microstructural Processes in Irradiated Materials, Boston, MA, 27–30 November, 2000, vol. 650, Materials Research Society, Pittsburgh, PA, 2001, R6.6.1.
[32] Y.A. Nikolaev, JAI 4 (2007) (Paper ID JAI100695).
[33] G.R. Odette, P.M. Lombrozo, R.A. Wullaert, in: F.A. Garner, J.S. Perrin (Eds.), Effects of Radiation on Materials: 12th International Symposium, ASTM STP 870, American Society for Testing and Materials, 1985, pp. 840.
[34] R.K. Nanstad, R.G. Berggren, in: F.A. Garner, J.S. Perrin (Eds.), Effects of Radiation on Materials: 16th International Symposium, ASTM STP 1175, American Society for Testing and Materials, Philadelphia, 1993, p. 239.
[35] M.A. Sokolov, R.K. Nanstad, in: R.K. Nanstad, M.L. Hamilton, F.A. Garner, A.S. Kumar (Eds.), Effects of Radiation on Materials: 18th International Symposium, ASTM STP 1325, American Society for Testing and Materials, West Conshohocken, PA, 1999, p. 167.
[36] P. Auger, P. Pareige, M. Akamatsu, J.-C. Van Duysen, J. Nucl. Mater. 211 (1994) 194.
[37] J.M. Hyde, D. Ellis, C.A. English, T.J. Williams, in: S. Rosinski, M.L. Grossbeck, T.R. Allen, A.S. Kumar (Eds.), Effects of Radiation on Materials, 20th International Symposium, ASTM STP 1405, American Society for Testing and Materials, West Conshohocken, PA, 2001, pp. 262.
[38] M.G. Burke, R.J. Stofanak, J.M. Hyde, C.A. English, W.L. Server, Characterization of irradiation damage in A508 Gr4N Forging Steels, in: Proceedings of 10th International Conference on Environmental Degradation of Materials in Nuclear Power Systems – Water Reactors, Lake Tahoe, NV, 5–9 August, 2001, NACE, 2002 (Electronic only).
[39] M.G. Burke, R.J. Stofanak, J.M. Hyde, C.A. English, W.I. Server, JAI 1 (2004) 194 (Paper ID JAI11773).
[40] M.G. Burke, M. Watanabe, D.B. Williams, J.M. Hyde, J. Mater. Sci. 41 (2006) 4512.
[41] P. Auger, S. Welzel, D. Blavette, P. Pareige, Radiation enhances segregation of impurities in ferrite RPV steels: APT study, in: Proceedings of XXVI Moscow International ITEP School of Physics, 17–26 February, 1998, Moscow.
[42] G.R. Odette, T. Yamamoto, D. Klingensmith, Philos. Mag. 85 (2005) 779.
[43] R.E. Stoller, The influence of damage rate and irradiation temperature on radiation induced embrittlement in pressure vessel steels, in: A.S. Kumar, D.S. Gelles, R.K. Nanstad, E.A. Little (Eds.), Effects of Radiation on Materials, ASTM STP 1175, ASTM International, West Conshohocken, PA, 1993, p. 394.
[44] T. Williams, D. Ellis, W. O'Connell, Dose rate effects in high and low nickel welds, in: Proceedings of the Workshop on Dose Rate Effects in Reactor Pressure Vessel Materials, Olympic Valley, CA, 12–14 November, 2001.
[45] K. Fujii, K. Fukuya, T. Ohmubo, K. Hono, T. Yoshiie, Y. Nagai, M. Hasegawa, in: Proceedings IGRDM 12, Arcachon, France, 2005 (unpublished).
[46] M.K. Miller, R.E. Stoller, K.F. Russell, J. Nucl. Mater. 230 (1996) 219–225.
[47] G.R. Odette, T. Yamamoto, B.D. Wirth, in: N.M. Ghoniem (Ed.), Proceedings of 2nd International Conference on Multiscale Materials Modeling, University of California, 2004, p. 355.
[48] G.R. Odette, in: I.M. Robertson, L.E. Rehn, S.J. Zinkle, W.J. Phythian (Eds.), Proceedings of MRS 1995 Meeting, Microstructure of Irradiated Materials, vol. 373, 1995, p. 137.
[49] G.R. Odette, G.E. Lucas, in: N.H. Packan, R.E. Stoller, A.S. Kumar (Eds.), Effects of Radiation on Materials, ASTM STP 1046, American Society for Testing and Materials, Philadelphia, PA, 1990, p. 323.
[50] A. Lambourne, D. Ellis, T. Williams, in: Proceedings IGRDM 13, Japan, 2006 (unpublished).